AD-A235 266

30 APR 1991

DOCUMENTATION PAGE

Form Approved OMB No. 0704-0188

UNCLASSIFIED	1b. RESTRICTIVE MARKINGS
2a. SECURITY CLASSIFICATION AUTHORITY	3. DISTRIBUTION/AVAILABILITY OF REPORT: Approved for public release; Distribution is unlimited
2b. DECLASSIFICATION/DOWNGRADING SCHEDULE	
4. PERFORMING ORGANIZATION REPORT NUMBER(S)	5. MONITORING ORGANIZATION REPORT NUMBER(S): AFOSR-TR- 91 0481
6a. NAME OF PERFORMING ORGANIZATION: Massachusetts Inst. of Tech.	6b. OFFICE SYMBOL (If applicable):
6c. ADDRESS (City, State, and ZIP Code): Haystack Observatory, Cambridge, MA 02139	7a. NAME OF MONITORING ORGANIZATION: AFOSR/NC
	7b. ADDRESS (City, State, and ZIP Code): Building 410, Bolling AFB, DC 20332-6448
8a. NAME OF FUNDING/SPONSORING ORGANIZATION: AFOSR	8b. OFFICE SYMBOL (If applicable): NC
	9. PROCUREMENT INSTRUMENT IDENTIFICATION NUMBER: AFOSR-89-0454
8c. ADDRESS (City, State, and ZIP Code): Building 410, Bolling AFB, DC 20332-6448	10. SOURCE OF FUNDING NUMBERS

PROGRAM ELEMENT NO.	PROJECT NO.	TASK NO.	WORK UNIT ACCESSION NO.
61102F	2310	A2	

11. TITLE (Include Security Classification): Storm Time Electric Field Penetration Observed at Mid-Latitude.

12. PERSONAL AUTHOR(S): H. -C. Yeh, J. C. Foster, F. J. Rich and W. Swider

13a. TYPE OF REPORT	13b. TIME COVERED	14. DATE OF REPORT (Year, Month, Day)	15. PAGE COUNT
Reprint	FROM _____ TO _____	April 1, 1991	15

16. SUPPLEMENTARY NOTATION: Journal of Geophysical Research, Vol. 96, No. A4, Pages 5707-5721, April 1, 1991.

17. COSATI CODES			18. SUBJECT TERMS (Continue on reverse if necessary and identify by block number)
FIELD	GROUP	SUB-GROUP	Radar, magnetosphere, DMSP

19. ABSTRACT (Continue on reverse if necessary and identify by block number)

Under disturbed geomagnetic conditions the latitudinal profile of the westward ion convection (equivalent to poleward electric field) observed with the Millstone Hill incoherent scatter radar at dusk, often exhibits a double peak (dual maxima). During the height of the February 8-9, 1986, magnetic storm the Millstone Hill radar was in the evening local time sector (1600-2200 MLT). Radar observations indicate that high speed (>1000 m s−1) westward ion flow penetrated deeply below 50° invariant latitude (Λ) and persisted for 6 hours between 2100 UT on February 8 and 0300 UT on February 9. The double-peaked ion convection feature was pronounced throughout the period, and the separation in the dual maxima ranged from 4° to 10°. The latitude positions of the high-latitude ion drift peak and the convection reversal varied in unison. The low-latitude ion drift peak (~49°Λ or L=2.3) did not show significant universal time/magnetic local time (UT/MLT) variation in its latitude location but showed a decrease in magnitude during the initial recovery phase of the storm. Using simultaneous particle (30 eV - 30 keV) precipitation data from the DMSP F6 and F7 satellites, we find the high-latitude ion drift peak to coincide with the boundary plasma sheet/central plasma sheet transition in the high ionospheric conductivity (>15 mho) region. The low-latitude ion drift peak lay between the equatorward edges of the electron and soft (< 1 keV) ion precipitation in the low conductivity region (~1 mho). A comparison between the low-altitude observations and simultaneous ring current observations from the high-altitude AMPTE satellite further suggests that the low-latitude ion drift peak is closely related to the maximum of the O+ dominated ring current energy density in magnetic latitude. The low-latitude ion drift peak is the low-altitude signature of the electric field shielding effect associated with ring current penetration into the outer layer of the storm time plasmasphere. Unlike the transient and localized subauroral ion drifts under moderately disturbed conditions, the intense westward ion drifts developed in response to heavy ion ring current shielding during a great magnetic storm can decouple from the high-latitude electric field and penetrate to very low latitudes and persist for long durations in the dusk and early afternoon MLT sectors. These features confirm the active role of storm time ring current dynamics in generating the low-latitude extension of the magnetospheric electric field.

20. DISTRIBUTION/AVAILABILITY OF ABSTRACT	21. ABSTRACT SECURITY CLASSIFICATION
☐ UNCLASSIFIED/UNLIMITED ☐ SAME AS RPT ☐ DTIC USERS	UNCLASSIFIED
22a. NAME OF RESPONSIBLE INDIVIDUAL: J G STOBIE, Lt Col, USAF	22b. TELEPHONE (Include Area Code): (202) 767-4960
	22c. OFFICE SYMBOL: AFOSR/NC

DD Form 1473, JUN 86 — Previous editions are obsolete. SECURITY CLASSIFICATION OF THIS PAGE: UNCLASSIFIED

DTIC FILE COPY

91 5 07 008

JOURNAL OF GEOPHYSICAL RESEARCH, VOL. 96, NO. A4, PAGES 5707–5721, APRIL 1, 1991

Storm Time Electric Field Penetration Observed at Mid-Latitude

H.-C. YEH AND J. C. FOSTER

Atmospheric Sciences Group, Haystack Observatory, Massachusetts Institute of Technology, Westford

F. J. RICH AND W. SWIDER

Space Physics Division, Geophysics Laboratory, Hanscom Air Force Base, Massachusetts

Under disturbed geomagnetic conditions the latitudinal profile of the westward ion convection (equivalent to poleward electric field) observed with the Millstone Hill incoherent scatter radar at dusk, often exhibits a double peak (dual maxima). During the height of the February 8-9, 1986, magnetic storm the Millstone Hill radar was in the evening local time sector (1600-2200 MLT). Radar observations indicate that high speed (>1000 m s^{-1}) westward ion flow penetrated deeply below 50° invariant latitude (Λ) and persisted for 6 hours between 2100 UT on February 8 and 0300 UT on February 9. The double-peaked ion convection feature was pronounced throughout the period, and the separation in the dual maxima ranged from 4° to 10°. The latitude positions of the high-latitude ion drift peak and the convection reversal varied in unison. The low-latitude ion drift peak (~49°Λ or L=2.3) did not show significant universal time/magnetic local time (UT/MLT) variation in its latitude location but showed a decrease in magnitude during the initial recovery phase of the storm. Using simultaneous particle (30 eV - 30 keV) precipitation data from the DMSP F6 and F7 satellites, we find the high-latitude ion drift peak to coincide with the boundary plasma sheet/central plasma sheet transition in the high ionospheric conductivity (>15 mho) region. The low-latitude ion drift peak lay between the equatorward edges of the electron and soft (< 1 keV) ion precipitation in the low conductivity region (~1 mho). A comparison between the low-altitude observations and simultaneous ring current observations from the high-altitude AMPTE satellite further suggests that the low-latitude ion drift peak is closely related to the maximum of the O^+ dominated ring current energy density in magnetic latitude. The low-latitude ion drift peak is the low-altitude signature of the electric field shielding effect associated with ring current penetration into the outer layer of the storm time plasmasphere. Unlike the transient and localized subauroral ion drifts under moderately disturbed conditions, the intense westward ion drifts developed in response to heavy ion ring current shielding during a great magnetic storm can decouple from the high-latitude electric field and penetrate to very low latitudes and persist for long durations in the dusk and early afternoon MLT sectors. These features confirm the active role of storm time ring current dynamics in generating the low-latitude extension of the magnetospheric electric field.

1. INTRODUCTION

Millstone Hill is optimally situated for observing phenomena associated with the plasmapause and the mid-latitude trough, but during magnetospheric disturbances its field of view encompasses middle and auroral latitudes as well as the polar cap boundary [*Yeh et al.*, 1990]. The magnetic storm of February 8-9, 1986, was one of the largest in the past decade. *Kp* reached 9 and the magnetopause was compressed to L=5.2 in the evening sector near 2100 UT on the 8th. The Millstone Hill incoherent scatter radar (MHR) (geodetic 42.6°N; 288.5°E; L=3) was operated in a storm survey mode, which included azimuth, and elevation scans and zenith observations, throughout the most disturbed storm period in response to an X1.7 solar flare which occurred at 0625 UT on February 6, 1986. The time evolution of the *Dst* and *Kp* indices for February 6 through February 10 is shown Figure 1. The times of interest (indicated by asterisks) are from 2100 UT February 8 to 0300 UT February 9, when *Dst* indicated the storm was near the main and early recovery phases. During these UT hours the MHR was in the evening magnetic local time (MLT) sector, a preferred MLT for the presence of partial ring current, and observed strong westward ion flows at very low latitudes (35°-45° geodetic). A 3-hour period of intense O^+ ion outflow at Millstone's latitude accompanied this storm maximum period and has been reported separately by *Yeh and Foster* [1990].

Figure 2 presents a comparison of a representative evening local time sector latitude profile of the east-west ion convection velocity observed at the February storm maximum, with those typical of less disturbed geomagnetic conditions. The data were taken with low elevation angle azimuth scans to the west of the site, at local times when the dominant convection direction is east-west [e.g., *Foster et al.*, 1986]. Line-of-sight (LOS) velocity corrected for the local magnetic westward direction cosine are presented. As the *Kp* level increases from 2 to 9, the spatial extent of the westward ion drifts (corresponding to northward electric field) widens (from 6° to 15°), and the equatorward edge of the drift region expands toward lower latitude (from 63°Λ (L=4.8) to 46°Λ (L=2.1)). Intense poleward electric fields at middle and low latitudes at dusk can effectively transport solar-produced plasma through the dayside cleft where it can become a source of enhanced ionization patches in the polar cap [*Foster*,

Paper number 90JA02751.
0148-0227/91/90JA-02751$05.00

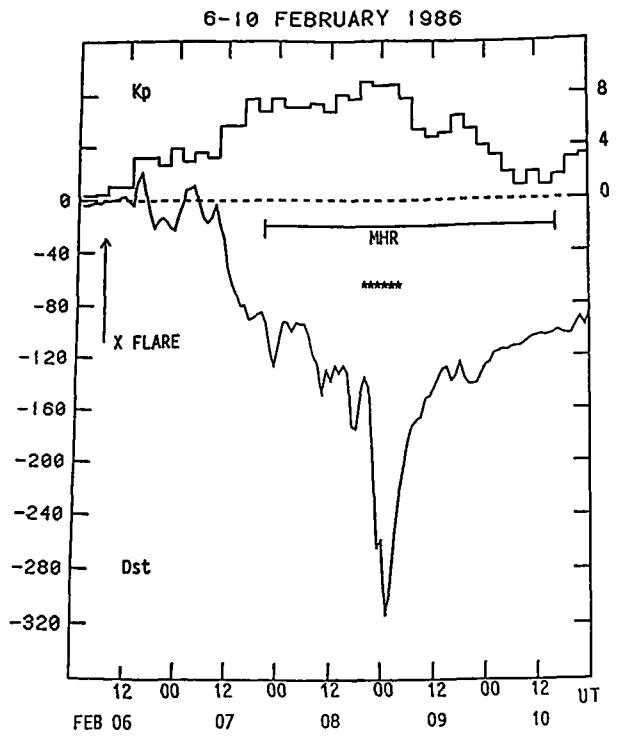

Fig. 1. Summary of *Kp* and *Dst* indices for February 6-10, 1986 UT. An X1.7 solar flare occurred at 0620 UT on February 6, 1986. The times of interest (indicated by asterisks) are from 2100 UT on the 8th to 0300 UT on the 9th, during which Millstone Hill Radar (MHR) was at evening local times, and observed intense westward ion drifts at low latitudes (below 50°Λ).

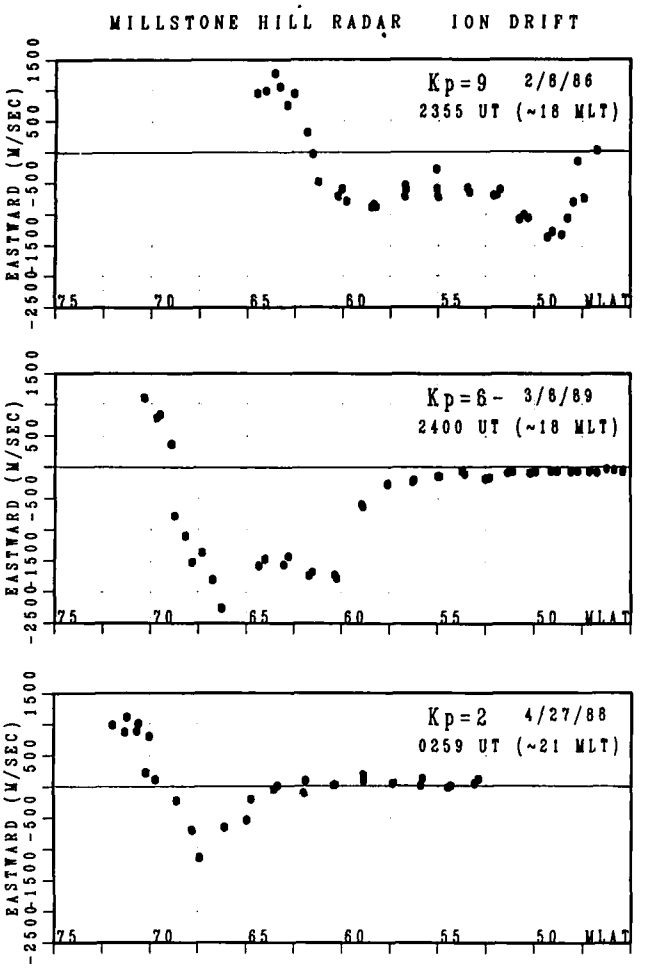

Fig. 2. Typical latitudinal profiles of the east-west ion convection velocities observed with the Millstone Hill incoherent scatter radar in the evening MLT sectors, for 3 *Kp* levels. The convection pattern shifts equatorward and expands as *Kp* increases. Dual maxima form as *Kp* reaches moderately disturbed conditions (*Kp*>4).

1989; *Foster et al.*, 1990]. In addition, intense ion convection in the collision-dominated region can result in strong and rapidly changing frictional heating which in turn can trigger heavy ion outflow [J. -P. St.-Maurice et al., unpublished manuscript, 1989; *Yeh and Foster*, 1990].

We observe that when geophysical conditions become moderately disturbed (*Kp*>5), the westward ion drift pattern exhibits a pronounced double-peaked feature. For the data of Figure 2 the latitudinal separation of the two peaks is ~7° for *Kp*=6−, and ~10° for *Kp*=9. Such a double-peaked feature was evident in the ion drift data for 6 hours during the maximum phase of the February storm. Magnetospheric plasma shielding and the ionospheric disturbance dynamo are the principal mechanisms which have been proposed to explain the electric field penetration to the mid- and low-latitude ionosphere during disturbed geophysical conditions. *Blanc and Richmond* [1980] have described the ionospheric disturbance dynamo which attributes the cause of the low-latitude electric field penetration to changes in the global thermospheric circulation produced by auroral heating during disturbed geomagnetic conditions. In this paper we examine concurrent low- and high-altitude particle populations in order to address the origin of the large-scale double-peaked ion convection structures.

Electric field shielding in the equatorial magnetosphere arises when the inward transport of injected plasma in the time varying magnetic and convection electric fields, and the corotation electric field, results in electron and ion separation and plasma pressure gradients [e.g., *Chen*, 1970; *Ejiri*, 1978; *Kivelson et al.*, 1979]. These couple to the ionosphere by particle precipitation [*Kennel*, 1969; *Southwood and Wolf*, 1978], ionospheric conductivity [*Wolf*, 1970; *Senior and Blanc*, 1984], and field-aligned currents [*Schield et al.*, 1969; *Vasyliunas*, 1972] to control the convection structure and prevent the convection electric field from further inward penetration. The complexity of these processes has been investigated in many simulation studies [e.g., *Harel et al.*, 1981; *Wolf et al.*, 1982; *Blanc*, 1983; *Spiro et al.*, 1988]. In examining the variations of the Saint-Santin (44.6°N; 2.2°E) *E*×*B* drifts during magnetic storms, *Blanc* [1978, 1983] found good correlation between the westward ion drift intensification and the large ring current inflation rate in the evening MLT sector, and suggested the active role of ring current dynamics in accounting for the low-latitude extension of the large-scale electric field structure. Thus, of particular interest to our present study is the shielding effect resulting from energetic ring current ion penetration into the inner magnetosphere.

Combining the observations from the Millstone Hill radar and the DMSP F6, F7 satellites at low altitudes, with those from the AMPTE satellite at the magnetospheric equatorial plane, we examine the effects of plasma shielding on the characteristics of the observed electric field. A close connection between the electric field structure and the shielding associated with ring current ion pressure and ionospheric conductivity gradients was found throughout the maximum phase of the February 8-9, 1986, magnetic storm.

2. RADAR OBSERVED ION DRIFTS AT 1500-2200 MLT

The radar azimuth scan has been used as a standard technique at Millstone Hill to provide wide latitude and local time coverage of the mid- and high-latitude ionosphere. By scanning the monostatic radar beam in azimuth at low elevation angle, Doppler returns indicating the line-of-sight component of the *F* region plasma motion are observed over a large range of latitude and longitude with approximate 30-min temporal resolution.

We have derived the two-dimensional ion convection patterns from the spline-fit technique [*Holt et al.*, 1984] for each of the successive azimuth scans between 2000 UT on February 8, and 0400 UT on February 9. Our electrostatic fitting program, which determines the electrostatic potential field that best fits the whole set of scan data, has a spatial resolution of 200 to 300 km which is set by the spline node separation and the density of observation points in the data grid. Detailed features of the convection pattern along a specific longitude (e.g., the satellite track) can be masked. This is particularly true for structures with sharp spatial gradients (such as the case we are treating). Nevertheless, these large-scale patterns consistently indicate that the ion drifts were largely confined in the east-west direction at the middle and low magnetic latitudes (below 60°). Hence we present only the east-west components of the ion drift velocities derived directly from our LOS observations and assume that they reveal the dominant characteristics of the underlying electric field patterns at these latitudes.

In order to make quantitative comparison with the high-resolution observations from the DMSP satellites, which moved approximately from north to south in the dusk to premidnight MLT sector, a latitude profile of the ion velocities with fine spatial resolution and with large latitude coverage is needed from the azimuth scan data. Since a line-of-sight drift is the quantity with the finest possible resolution, the line-of-sight ion drifts at a fixed altitude (thus along an approximately constant longitude) from single azimuth scans are used. The east-west component of the ion drift velocity is determined from the corresponding line-of-sight measurement corrected by its direction cosine with respect to the local magnetic field direction.

Figure 3 shows a comparison between the latitude profile of the east-west ion drifts derived from the MHR line-of-sight measurements using the above method, and that of the nearly simultaneous (within 5 min) east-west ion drifts directly measured by the drift meter of the DMSP F8 satellite. As seen in the figure, the double-peaked feature is evident in both sets of the observations. The latitudes of the peaks determined

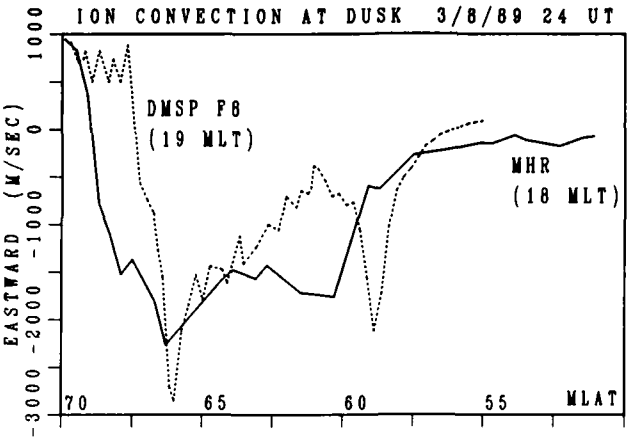

Fig. 3. Latitudinal profiles of the east-west ion convection derived from nearly simultaneous Millstone Hill radar line-of sight and the DMSP F8 satellite drift meter observations. Both instruments observed a double-peaked westward convection feature. The latitude difference in the two low-latitude peaks can be explained in terms of the longitude difference (~1.5 hour MLT) of the profiles.

from the radar and DMSP satellite agree well if we take into account the longitudinal difference (~1.5 hour MLT at ~60°) between the two sets of observation . As we expect, somewhat finer-scale structure is resolved in the satellite data and the radar LOS measurements somewhat underestimate the magnitude of the drift velocity due to spatial smearing. Unfortunately, similar confirmation can not be done for the February, 1986, events, since neither the DMSP F6 nor the DMSP F7 satellite carried a drift meter.

Figure 4 presents a series of ion convection patterns at 400-500 km altitude which illustrates the characteristic features of the ion convection during the height of the storm. These apex magnetic latitude (MLAT) profiles of the east-west ion convection velocity are derived from single 15-min azimuth scans during five selected UT intervals. These profiles are labeled chronologically according to the central time of each of the scans, as "A" to "E." The polar plot at the left top corner of Figure 4 delineates the positions of the radar measurements in apex magnetic latitude and magnetic local time coordinates for each scan.

During these UT intervals the radar observations were made in the 1600 to 2100 MLT sector. In all but the "E" panel (centered around 0212 UT on February 9), the ion drift patterns showed a pronounced double-peaked feature. In general, the ion drift speed exceeded 1000 m s^{-1} at the maxima, and did not penetrate below ~46° MLAT. The location of the high-latitude maxima varied between 55° and 59° MLAT. The location of the low-latitude peak was more confined, lying between 49° and 51° MLAT. Near 24 UT on the 8th (at storm maximum), there was a DMSP F6 pass within the Millstone Hill radar field of view. We use the ion drift pattern at this time, panel "C," to define several latitudinal boundaries for further discussion of the convection electric field patterns. These are: convection reversal (from eastward drift direction to westward) R; maximum westward drift at high latitude H; westward ion drift peak at low latitude L; local minimum

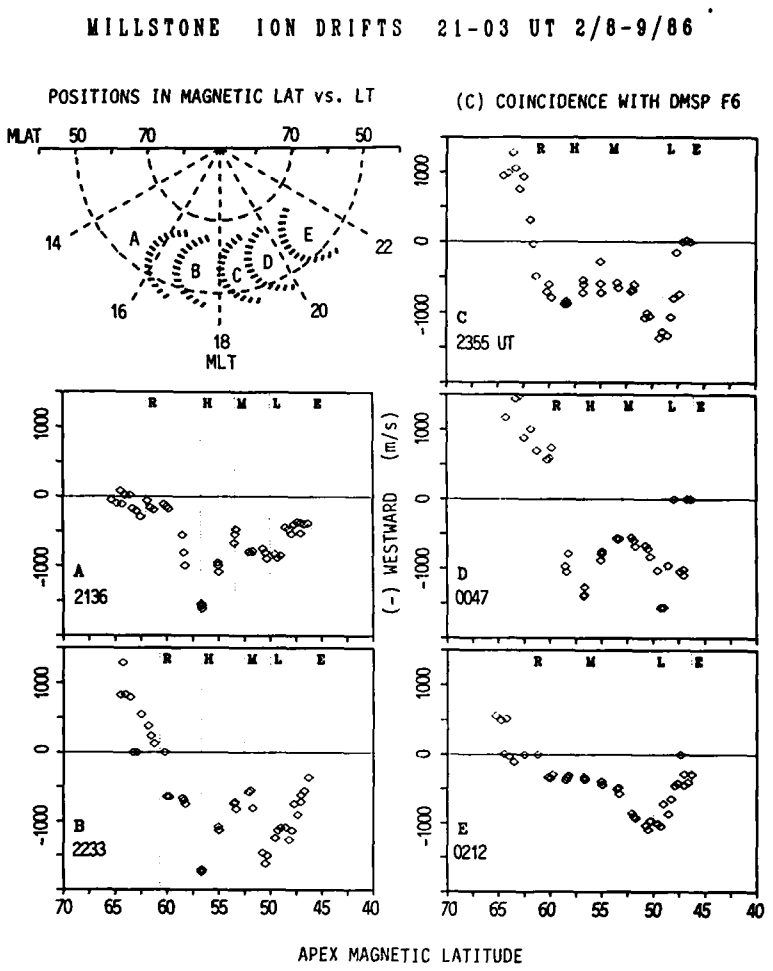

Fig. 4. Latitudinal ion drift patterns from individual radar azimuth scans at 5 different UT times between 2100 UT February 8 and 0300 UT February 9, 1986. The magnetic latitude-local time distribution of these scans is shown at the left-top panel. A double-peaked westward drift feature persisted throughout most of the period. The latitude locations of convection reversal (R), high-latitude westward ion drift peak (H), low-latitude westward ion drift peak (L), the minimum in between the two peaks (M), and the equatorward boundary (E) are indicated by the dashed lines.

between the two drift peaks M; equatorward boundary of the drift E. The uncertainty of E is large since it is located near the low boundary of an azimuth scan.

The latitudes of the above boundaries and their corresponding ion speeds for all successive scans from 2000 UT February 8, to 0400 UT February 9 are identified and shown in Figure 5. There were no double-peaked patterns observed before 2100 UT (1500 LT) and after 0300 UT (2100 LT). The ion drift measurements before 2100 UT were taken immediately following the strong IMF southward turning (at ~2013 UT) and were in the dayside where the solar produced conductivity may short out the localized electric field. The absence of the double-peaked ion drift pattern after 03 UT probably reflected the O^+ ring current decay during the initial recovery phase of the storm in combination with the MLT dependence. A few other features are apparent in Figure 5*b*. The latitude of the convection reversal (R) varied in unison with the high-latitude ion drift peak (H) and the minimum (M) throughout most of the 8-hour period. The low-latitude ion drift peak (L) was in its lowest position when the storm approached the maximum phase ($Dst = -312$ nT), and did not move back to higher latitudes as the other boundaries did at ~0140 UT on the 9th.

Figure 5*a* illustrates the temporal/local time variations of the convection speeds at the boundaries presented in Figure 5*b*. Before 2100 UT, westward convection, which maximized at H, gradually attenuated to zero with decreasing latitude. After 2100 UT a second drift maximum (L) appeared and its speed remained approximately constant (1200 to 1600 m s^{-1}), for 3 hours from 2200 to 0100 UT. The H's ion speeds were larger than those at the Ls for the intervals 2100 to 2330 UT on the 8th, and after 0230 UT on the 9th. The L's speed exceeded the H's speed from 2340 to 0230 UT, and decreased from >1200 to ~500 m s^{-1} during the period from 0100 UT to 0300 UT. The small speed at L before 2200 UT probably can be attributed to the higher ionospheric conductivity in the dayside MLT sector. The distinguishable temporal characteristics of the high- and low-latitude convection peaks provide us an additional clue

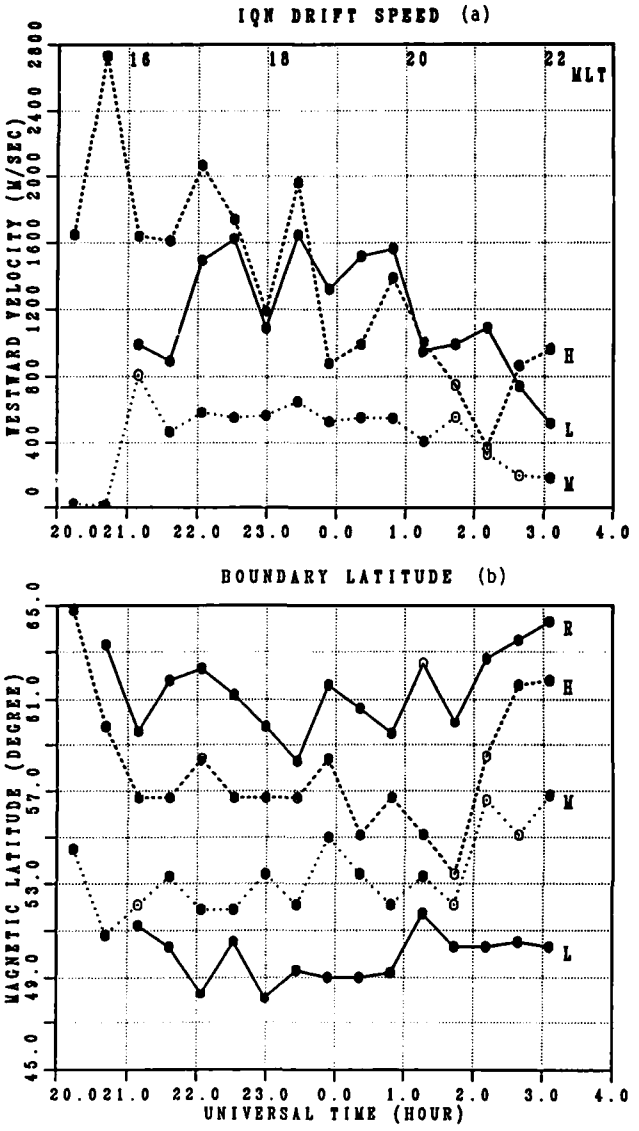

Fig. 5. (b) Temporal (UT) and MLT variations of the latitudes of R, H, M, and L (see text for definition of these notations); and (a) the drift speeds at H, M, and L derived from all radar scans from 2000 UT on February 8, 1986, to 0400 UT on February 9, 1986. Open circles indicate less confident estimates. Significant changes in the R, H, and M latitudes and in the H speed occurred at >0140 UT on the 9th.

regarding the origin of the two peaks. We will discuss this point in more detail in the following sections.

3. Relationship to Particle Precipitation

The equatorward boundaries of the auroral precipitation at the dawn, noon, dusk, and midnight sectors for the three most disturbed days (7-9) of February 1986 have been studied by *Swider* [1990] using particle observations from the DMSP F6 and F7 satellites at ~840 km altitudes. In this paper we concentrate on the spectral details of the dusk-midnight particle precipitation patterns observed by the DMSP satellites during the time interval (2000 UT on February 8 to 0400 UT on February 9), during which the double-peaked ion convection patterns were observed.

Particle precipitation can significantly modify the convection electric field structure by changing the conductivity distribution in the ionosphere and by disrupting the shielding in the inner equatorial magnetosphere [*Kennel*, 1969; *Southwood and Wolf*, 1978]. In this section we investigate the latitudinal relationship between the radar-observed ion drifts and the low-altitude satellite-observed particle precipitation patterns. Figure 6 depicts the footprint of the DMSP satellite orbit and the location of the MHR observations in apex magnetic latitude/magnetic local time coordinates for two time intervals during which the satellite and radar observations were nearly coincident. Figure 6*a* shows the event on February 8-9, 1986, including the DMSP F6 orbit from 2350 UT on the 8th to 0004 UT on the 9th, and the radar observations which extended from 2349 to 2359 UT on the 8th. Figure 6*b* shows the event on

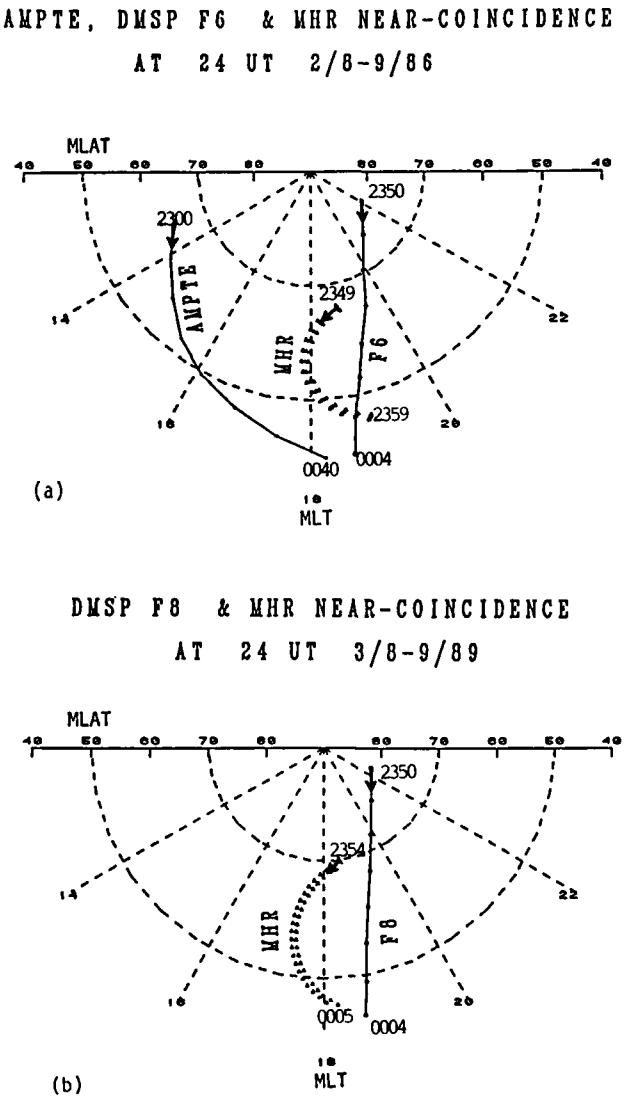

Fig. 6. Satellite (AMPTE and DMSP) orbits and Millstone Hill radar (MHR) observations in apex magnetic latitude and local time coordinates for two near-coincident (UT) events. The start and end UT times of the plotted satellite trajectories and of the radar scan are indicated in the figures. (*a*) AMPTE, DMSP F6 and MHR coincidence on February 8-9, 1986; (*b*) DMSP F8 and MHR coincidence on March 8-9, 1989.

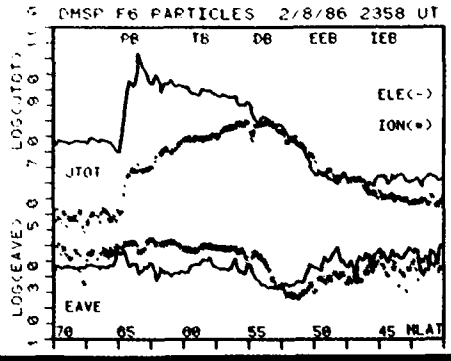
DMSP F6 PARTICLES 2/8/86 2358 UT
PB TB DB EEB IEB
ELE(-)
ION(+)
JTOT
EAVE
LOG(JTOT)
LOG(EAVE)
70 65 60 55 50 45 MLAT

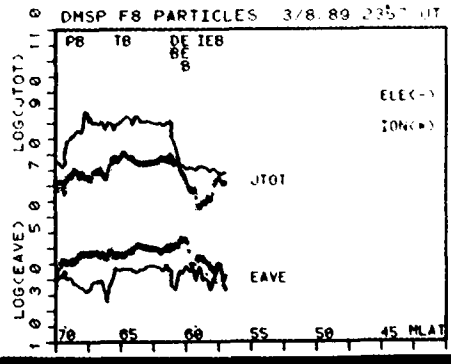
DMSP F8 PARTICLES
PB TB DE IEB
ELE(-)
ION(+)
JTOT
EAVE
LOG(JTOT)
LOG(EAVE)
70 65 60 55 50 45 MLAT

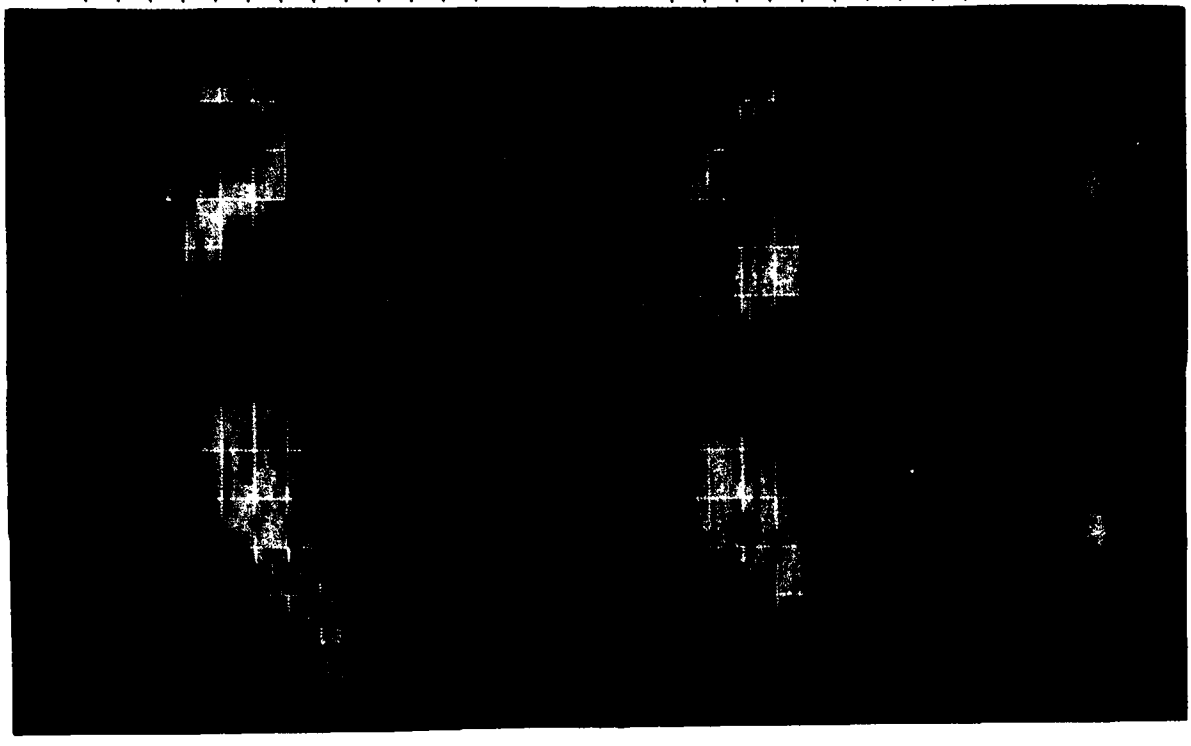

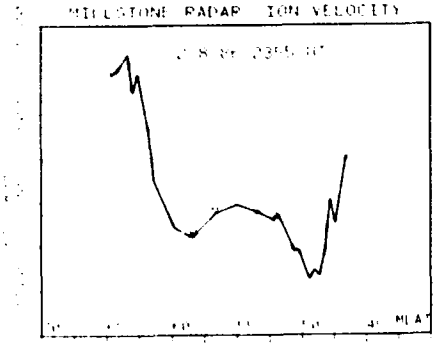
MILLSTONE RADAR ION VELOCITY
MLAT

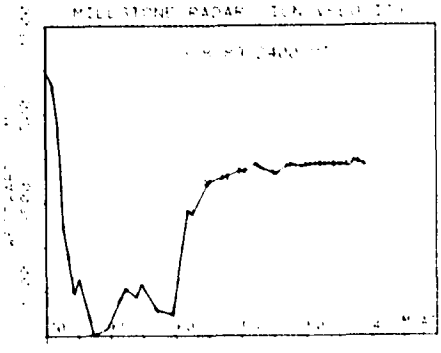

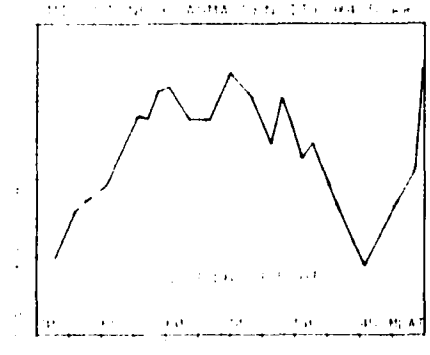
MLAT

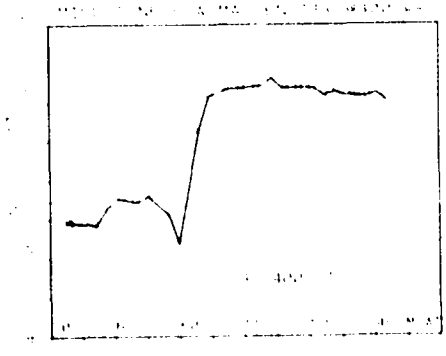

March 8-9, 1989, for a less disturbed condition (Kp=6−), including the DMSP F8 orbit from 2350 UT March 8 to 0004 UT March 9, and the radar observations during 2354 UT on March 8 to 0005 UT on March 9. Figure 6 indicates that the local time coincidence between the DMSP satellite and radar observations was good (<1.5 hour difference) for both events. Of particular interest is the nearly perfect coincidence between the satellite and the radar observations at about 50° MLAT for the February 1986 storm.

In Plate 1 the latitude variation of the precipitating electrons and ions from the satellite observations and the east-west component of the ion drift and plasma density at ~450 km altitude from the radar observations are plotted. Particle patterns, including the integrated (over 30-eV to 30-keV energy range) directional number flux (JTOT in particles cm^{-2} s^{-1} sr^{-1}), the average energy (EAVE in eV), and the latitude-energy-directional energy flux (EFLUX in eV cm^{-2} s^{-1} sr^{-1}) spectrograms for electron and ion, are displayed in the top three panels. The ion convection pattern and the F region plasma density distribution are shown at the bottom panels for comparison. The latitudinal profiles of particle precipitation, ion drift, and plasma density for the March 8-9, 1989, event are displayed to the right.

We examine the particle patterns for the February 8-9, 1986, event first, to locate the various boundaries which delineate the characteristic plasma regions. The poleward boundary (PB) of the electron flux enhancement was found to be collocated with that of the ion flux enhancement at ~64.9° MLAT. The electron flux falls to its background level at ~50.4° MLAT (L=2.5) which marks the equatorward boundary of the electron flux enhancement (EEB). Significant ion precipitation was seen equatorward of the EEB and the ion equatorward boundary (IEB) was found at 45.8° MLAT (L=2.1). Based upon the particle spectral features, we further identify the other two characteristic boundaries: the transition boundary (TB), at 58.8° MLAT, which separates the boundary plasma sheet (BPS) population [*Winningham et al.*, 1975] on the higher latitude side from the central plasma sheet (CPS) population [*Winningham et al.*, 1975] on the lower latitude side; and the dispersion boundary (DB) at 54.7° MLAT, which marks the highest latitude location of the particle energy-latitude dispersion structure (particle flux and/or average energy decreases with decreasing latitude) and may be used to delineate the equatorward edge of the conductivity produced by hard precipitating electrons.

Comparing these particle boundaries with the ion convection pattern, the following features are noteworthy. The convection reversal R is about 1°-2° equatorward of the poleward boundary PB. The transition boundary (TB) approximately coincides with the high-latitude ion drift peak (H at 58.4° MLAT). The particle dispersion boundary (DB) is approximately collocated with the minimum westward ion drift (or the weakest N-S electric field) between H and L. The low-latitude ion drift peak (L at ~49° MLAT) lies between the electron and ion equatorward boundaries. Thus from the morphological point of view, the ion drift at L can be classified as a subauroral ion drift. The equatorward limit E of the ion drift approximately coincides with the precipitating ion equatorward boundary.

The minimum (N_e=10^4 cm^{-3}) of the plasma density trough is located (45° MLAT) further equatorward of the edges of both ion precipitation and ion drifts (see bottom panels). The 5.4° equatorward displacement of the plasma density trough from the plasma sheet electron EEB is comparable to those reported by *Foster et al.* [1978]. They investigated plasmapause signatures in the ionosphere and magnetosphere and found that the invariant latitudes of the ionospheric plasma troughs are height dependent such that at low altitudes, in the pre-midnight sector the trough often begins 2°-10° equatorward of the field line through the equatorial plasmapause. They found that the low-latitude extent of the plasma sheet electrons is a better signature than the ionospheric trough of the equatorial plasmapause position. If we adopt the invariant latitude of EEB as the approximate position of the equatorial plasmapause, the plasmapause of the February 8-9 event then is located at ~L=2.5 (50.4° Λ) at 19 MLT. This is a much larger equatorial distance than that (L=1.7) found by *Swider* [1990] at dawn. Since time varying convection on scale of hours can result in complex fine structure in the outer plasmasphere at dusk MLT [*Wolf et al.*, 1986, and references therein], we do not expect a well-defined plasmapause position during the time interval of interest.

Another interesting feature is the significant latitude separation (4°) of the low-latitude ion drift peak from the center of the plasma trough during the February storm maximum. This contrasts to the findings of *Senior et al.* [1987] for moderately disturbed conditions, who reported intense (50 mV m^{-1}) northward electric field (westward convection) extending below the plasma trough latitude. The magnetic activity dependence of the relative location between convection electric field and plasma trough is worthy of investigating in the future.

The particle boundaries: PB, TB, DB, EEB, and IEB are also identified and compared with the latitudinal profiles of the ion drift and thermal plasma density for the less severely disturbed March 8-9, 1989, event. Enhanced particle fluxes were seen at much higher latitudes and spanned a narrower spatial extent (57°-69.3° MLAT) than those of the February 8-9, 1986, event. The electron and ion equatorward boundaries are located at 60.5° and 59.3° MLAT (L=4.1-3.8), respectively. The

Plate 1. (Opposite) Apex magnetic latitude variation of simultaneous radar (at ~450 km altitude) and DMSP satellite (at ~840 km altitude) observations at dusk MLT. 30 eV to 30 keV precipitating particle flux (JTOT, in particles cm^{-2} s^{-1} sr^{-1}), average energy (EAVE, in eV), electron and ion differential energy flux spectrograms (EFLUX in eV cm^{-2} s^{-1} sr^{-1}), and the radar observed ion convection and F region plasma density, are shown from top to bottom. February 1986 event (Kp=9) on the left; March 1989 event (Kp=6−) on the right. PB denotes particle poleward boundary, TB the BPS/CPS transition, DB the poleward edge of energy-latitude dispersion, EEB (IEB) the electron (ion) equatorward boundary. The high-latitude westward convection peak was collocated with TB, and the low-latitude peak lay between EEB and IEB.

separation between EEB and IEB is much less than that (>4°) of February 8-9 event at the lower latitudes (L=2.1-2.5).

In addition to morphological differences between the two events the particle precipitation of the March 8-9 event is generally an order of magnitude weaker and less energetic than that of the February 8-9 event. The color bar scales in Plate 1 for the two events are offset by an order of magnitude in order to compensate for this difference. The spectral difference between the two events is particularly clear in the electron-BPS region (between PB and TB) which we will call the outer magnetospheric region to be distinguished from the inner magnetosphere of the CPS. For the March 8-9 event the 500-eV to 2-keV electrons dominated the energy flux in the BPS region, while the 1- to 3- keV electrons are the major component in the CPS region. This spectral difference between BPS and CPS is typical [*Winningham et al.*, 1975]. However, the 3 to 10 keV (comparable to the average electron energy in CPS) electrons were greatly enhanced in the BPS region during the February 8-9 event. The particle energy input to the outer magnetosphere for the February 8-9 event was extremely high.

In spite of significant differences in the particle precipitation patterns between the two events, a similar latitudinal relationship between the particle boundaries and the double-peaked ion drift pattern is found. For the March 8-9 event the DMSP F6 drift meter also measured the ion convection pattern. Both the ion drift patterns from the satellite and from the radar measurements show double-peaked characteristics [*Foster et al.*, 1989; Figure 3]. Again, the high-latitude ion drift peak collocates with the BPS/CPS transition boundary and the low-latitude ion drift peak from the satellite falls between the electron and ion equatorward boundaries. The low-latitude ion drift peak of the March 8-9 event is spatially close to the minimum of the plasma trough and is narrower than that of the stronger February 8-9 event.

4. Electric Field Shielding Effects

In the inner magnetosphere and low-latitude ionosphere the ring current energy density (pressure) and the ionospheric conductivity distributions [*Swift*, 1967; *Wolf*, 1970; *Vasyliunas*, 1970, 1972; *Southwood and Wolf*, 1978; *Blanc*, 1978, 1983; *Siscoe*, 1982] are the two most important factors in determining the electric field structure through current continuity in the magnetosphere-ionosphere system. The interplay of these factors has been commonly adopted to explain very intense, spatially localized, subauroral ion drifts [*Smiddy et al.*, 1977; *Spiro et al.*, 1979; *Rich et al.*, 1980; *Providakes et al.*, 1989]. We present here for the February 8-9 event a detailed comparison of the ion convection pattern with the conductivity and ring current ion pressure patterns.

Vasyliunas [1972] has suggested the important role of the ring current particle content in determining the convection pattern and proposed a parameter Σ^*/Σ^H to quantify the ring current shielding effect in the ring current-ionosphere coupling. Σ^* is eN, where N is the constant number of ring current particles in a flux tube enclosing unit magnetic flux [*Siscoe*, 1982]. In the electrical circuit representations of ring current-ionosphere coupling, Σ^* plays the role of a height-integrated Hall conductivity for the ring current. The corresponding magnetospheric Hall current flows in parallel with the ionospheric Hall current (with Hall conductivity Σ^H) to provide overall current continuity. In a region where Σ^*/Σ^H is large, ring current particles play a dominant role in determining the magnetospheric electric field structure.

4.1. Ionospheric Conductivity

Ionization in the nightside ionosphere principally results from energetic particle precipitation. Using *Robinson et al.* [1987] formulas, we estimate the height-integrated Hall (Σ^H) and Pedersen (Σ^P) conductivities from the electron ($\geq$ 500 eV) precipitation measured by the DMSP F6 SSJ/4 detector [*Hardy et al.*, 1984], and shown in the middle panel of Figure 7. The conductivity profiles show a high conductivity (>10 mhos) region associated with hard electron precipitation (see particle energy spectrum in Plate 1 at the latitudes above 55° MLAT). The large negative conductivity gradient at/near the convection reversal implies that a large field-aligned current is required in this location to complete current continuity.

Ion precipitation can also contribute significantly to E region ionization and conductivities [*Basu et al.*, 1987; *Senior et al.*, 1987]. We do not attempt to calculate the conductivities contributed by the ion precipitation since ion JTOT was generally an order of magnitude lower than electron JTOT above 55° latitude and energetic ion (>1 keV) precipitation was weak below 51.5° MLAT (see Plate 1 top panels). At the bottom panel of Figure 7 we include the latitude profile of the E region electron density derived from radar measurements for the same time interval to show the combined effect of ion and electron precipitation on ionization. From Plate 1 and Figure 7 it is evident that the intense energetic ion precipitation has contributed greatly to E region ionization in the latitude range between 55° and 51.5° MLAT. Consideration of electron precipitation alone would underestimate the magnitude of conductivity in this latitude range.

Comparing the ion convection pattern shown in the bottom panel of Figure 7, with the conductivity profiles, we see that the high-latitude ion drift peak is closely related to a sharp conductivity increase at the equatorward edge of the BPS precipitation. At these latitudes (61°-57°) the electron spectra (see Plate 1) were characterized by intense fluxes concentrated in a narrow energy range around 5 keV. This spectral feature indicates the presence of field-aligned potential drops in these latitudes. When large field-aligned currents develop in response to large potential gradients (or electric fields) in the magnetosphere, field-aligned potential drops occur which accelerate the field-aligned current carriers and create the ionospheric conductivity needed to complete the circuit from the magnetospheric generator. Thus in this region the electric field (convection velocity) pattern varies in unison with the conductivity changes to transmit field-aligned currents.

In the region equatorward of the large-scale field-aligned potential drop structure, from 57° to 51.5° MLAT, the conductivity resulting from particle precipitation was still high and conductivity enhancements on the scale size of an auroral arc (~0.5°) occurred at ~56° and 55° latitude. Because of intense particle precipitation and the resultant enhanced ionospheric ionization which supplies the upward flowing

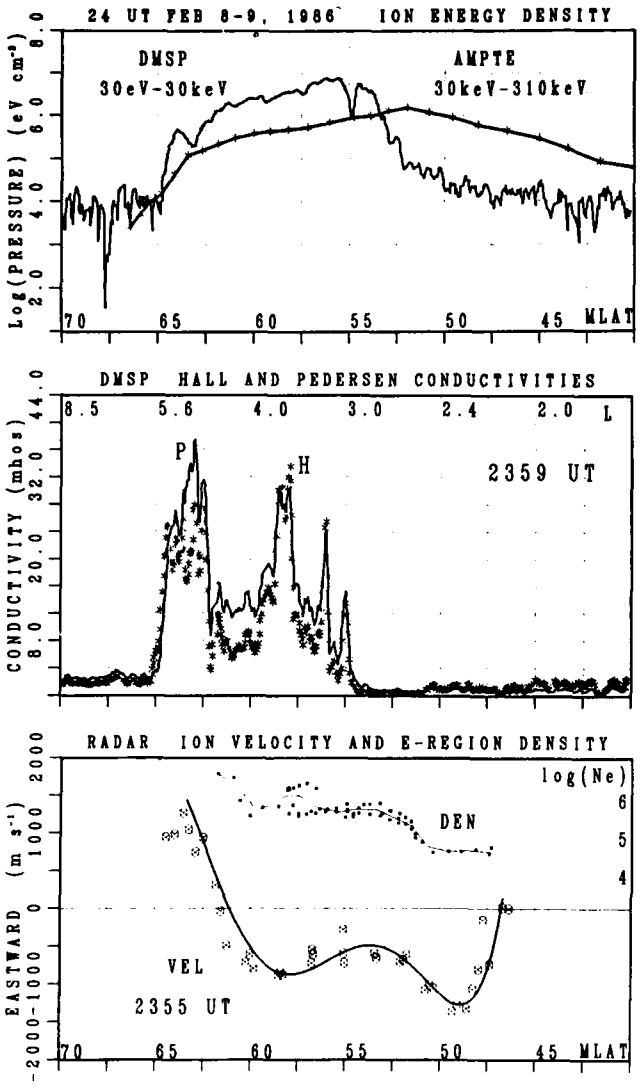

Fig. 7. (Top) Latitude distribution of ion ring current energy density. The ion energy density in 30-eV to 30-keV range is derived from the DMSP precipitating ions assuming an isotropic distribution. The energy density measured by AMPTE in the 30- to 310-keV range (line with asterisks) is the sum of H^+ and O^+ taken from *Hamilton et al.* [1988]. (Middle) Height integrated Hall (asterisks) and Pedersen (line) conductivities were derived from the DMSP F6 precipitating electrons with energy >500 eV. (Bottom) East-west ion convection velocity inferred from MHR line of sight ion drift and E region electron density profile showing ionization enhancements produced by particle precipitation. The low-latitude ion convection peak is in the low conductivity region and is driven by the energetic ring current pressure.

thermal electrons to carry return currents to the magnetosphere, the polarization electric field due to charge separation can not be effectively generated in such a region [*Schield et al.*, 1969]. *Southwood and Wolf* [1978] suggested that particle precipitation significantly reduces the effectiveness of the shielding of the inner magnetosphere from high-latitude electric field penetration. Thus the electric field shielding, as evidenced by the decrease in field strength with decreasing latitude, is gradual, in this high conductivity region. The embedded fine-scale conductivity enhancements can also cause the northward electric field to decrease with conductivity increases at 56° and 55° latitudes [*Doyle et al.*, 1986, and reference therein].

A significantly large electric field (≥25 mV m^{-1}), and resultant plasma convection velocity >500 m s^{-1}, extends equatorward of the high conductivity region and spans a large latitude range (51.5°-47° MLAT). To explain this low-latitude electric field, we examine the precipitating particle dispersion characteristics and the ring current ion distribution observed by the equatorial AMPTE satellite [*Hamilton et al.*, 1988].

4.2. *Ring Current Considerations*

In the equatorial magnetosphere, plasma is transported earthward from the nightside plasma sheet or geomagnetic tail regions under the combined effects of the convection, corotation, magnetic gradient drifts [e.g., *Kavanagh et al.*, 1968; *Chen*, 1970, *Ejiri*, 1978] and particle loss processes such as pitch angle diffusion [*Kennel*, 1969; *Southwood and Wolf*, 1978] and strong turbulent diffusion [*Cornwall et al.*, 1970]. These effects result in the dependence of the innermost position of the particle penetration on particle species, particle velocity distribution, and on the local time. In the dusk MLT sector a consideration of these effects predicts several features which are relevant to our observations. First, the ion and electron equatorward boundaries are expected to be separated, with the ion boundary extending to lower L values [*Gussenhoven et al.*, 1987]. Second, because the higher energy particles precipitate at a higher L region than the lower energy particles, an energy-latitude dispersion structure will be formed at the low-latitude extent of the particle precipitation region. As shown in the particle spectrograms of Plate 1, these predicted boundary features were clearly seen during the February 8-9, event [cf. *Swider*, 1990]. In addition, the medium energy ions, but not the electrons with comparable energy, can be driven by the convection electric field to penetrate to small radial distance (i.e., well inside the plasmapause), near the dusk meridian [*Chen*, 1970; *Cowley and Ashour-Abdalla*, 1976]. During the main phase of a geomagnetic storm the ions rapidly diffuse across the plasmapause and are lost before reaching the noon meridian [*Cornwall et al.*, 1970]. These phenomena give rise to an asymmetric ring current distribution, which then has an azimuthal pressure gradient and can drive field-aligned currents.

The shielding of the convection electric field from low-latitude flux tubes by pressure gradients at the inner edge of the ring current has long been recognized [*Vasyliunas*, 1972; *Jaggi and Wolf*, 1973]. *Southwood and Wolf* [1978] and also *Senior and Blanc* [1984] further examined the effects of the ionospheric conductivity on the shielding efficiency in terms of a shielding time scale, and a shielding factor which measures the spatial attenuation of the electric field. In the regions where plasma loss associated with strong particle precipitation dominates the charge exchange loss (i.e., in the outer magnetosphere, $L \geq 4$), Southwood and Wolf predicted that strong shielding should occur within the region between the ion and electron boundaries where the ion pressure and the conductivity gradients are the largest. Based on linear theory, *Senior and Blanc* [1984] predicted a time constant for the shielding effect on the order of 30 min or less. At or near the ring current inner boundary, pressure gradients drive azimuthal ion flows from the

nightside toward the dayside. Ring current energy is diverted into the ionosphere through field-aligned currents and subsequent ionospheric current closure in the low conductivity region. As a result of these processes, intense subauroral westward ion drifts are produced [e.g., *Rich et al.*, 1980; *Senior et al.*, 1987]. The narrower the charge separation (or the sharper the inner edge of ring current), the stronger the subauroral ion drift will be. The large low-latitude ion drift peak observed on March 8-9, 1989, during the moderately disturbed condition, is well described by the above processes.

In the dusk MLT sector the low-altitude signature of the electric field shielding effect associated with the asymmetric ring current distribution can well be characterized by the coincident intensification of the subauroral ion drift and the field-aligned current inside of the equatorward boundary of the precipitating plasma sheet electrons [*Rich et al.*, 1980; *Senior et al.*, 1987]. Unfortunately, the DMSP F6 and F8 satellites do not carry magnetometers, and the F7 satellite which does have a magnetometer, was traveling in the midnight MLT sector during the time interval of interest. Thus in the dusk MLT sector, relevant field-aligned current data are not available to compare with the simultaneous particle and electric field data in order to show such a relationship between the subauroral field-aligned current and the westward ion drift. Nevertheless, the magnetic field perturbations and particle precipitation patterns observed by the DMSP F7 satellite at ~2300 MLT, during the February 1986 storm maximum (~0035 UT on February 9) did reveal the existence of a significantly large (~2 μA m^{-2}) and structured (detached from the regular region 2 field-aligned current) field-aligned current sheet equatorward of the energetic CPS electron precipitation. This may be indicative of the longitudinal extent of the azimuthal ring current pressure gradient and/or of the low-latitude electric field intensification to ~2300 MLT. Again, due to the complicated nature of the midnight field-aligned current structure and the lack of electric field data at this MLT, we are not able to confirm this suggestion.

4.3. Ring Current Observations

In the following we examine the ring current pressure distribution near the main phase of the February 8-9, 1986, storm. Using Figure 1 of *Hamilton et al.* [1988], the AMPTE CCE trajectory for the inbound pass during 2300-0040 UT on February 8, 1986, is described in terms of invariant magnetic latitude and magnetic local time coordinates and shown in Figure 6*a* for comparison with the low-altitude observations by the Millstone Hill radar and the DMSP satellites. Figure 6*a* shows good UT coincidence among the AMPTE satellite, Millstone Hill radar, and DMSP F6 satellite at latitudes between 45° and 55° MLAT, though the AMPTE observations were made 2 hours earlier in MLT than the low-altitude observations. Similarly, the radial profile of the ring current energy density (a sum over the two major species: H^+ and O^+, taken from Plate 1 of *Hamilton et al.* [1988]) is transformed into a latitude profile for comparison with the latitude profiles of the low-altitude observations and shown at the top panel of Figure 7.

Before comparing the high-altitude and low-altitude observations we should comment on the uncertainty in determining the latitude profiles of the AMPTE observations. Because none of the existing quantitative models of the magnetospheric magnetic field [*Tsyganenko*, 1990] is applicable to the geophysical condition of the February, 1986, storm (Kp=9 with the heavy ion dominated ring current maximum located as close as 2-3 R_E), and because a more realistic magnetic field model can not be readily developed, we have used the simplest dipolar magnetic field model to do mapping. At the inner edge of the ring current distribution (2-3 R_E), deviation from the dipolar magnetic field configuration likely results from the ring current induced magnetic field. Since the L value used by *Hamilton et al.* [1988] as a radial distance parameter was calculated based on a quiet time magnetic field model, the invariant latitudes derived from their L values can only be treated as an approximation of their corresponding storm time magnetic latitudes. For general purposes, we have used a dipolar magnetic field mapping to relate L and our magnetic latitude throughout this paper.

The AMPTE observations during this storm-maximum pass indicate that the maximum in ring current energy density (integrated from 30 to 310 keV) moved inward to L=2.6 (51.6° Λ) and that the inner edge of the ring current distribution penetrated to $L \leq 2$ (45° Λ). The energy density of O^+ exceeded that of H^+ over the radial distance L=2.2-5.7 (47.5°-65° Λ). The O^+ energy spectrum peaked at about 30 keV in the L range 3-5. The low-energy ions (1 to 30 keV/*e*) contributed only about 5% of the total energy content in the L=2-3 range. We have estimated the energy density contribution of the low-energy ring current particles from the DMSP F6 ion precipitation (30 eV to 30 keV), assuming isotropic low-energy ions in the equatorial plane. This is shown in Figure 7 at the top. Comparing the ion drift profile with the ion pressure profiles from both the DMSP and AMPTE satellites, we find that the westward ion drift peaked in the low conductivity region, at a latitude where the low-energy ion density reached the background level and the energetic ring current pressure was decaying from its maximum.

A close inspection of the February 8 low-latitude (45°-55° MLAT) precipitating ion spectra presented in the Plate 1 and further detailed in Figure 8, reveals a spectral transition near 50° MLAT (~L=2.4). If the spectral transition in the ion precipitation pattern marks the plasma density change in the equatorial magnetosphere, or more specifically, the spectral transition marks the plasmapause, then the weaker and principally low energy ($\leq$ 1 keV) ion precipitation is consistent with being heated plasmaspheric ion precipitation. The heated ion spectrum at 49° in Figure 8 can be approximated by a Maxwellian distribution function with a temperature and density of about 120 eV and 30 cm^{-3}, respectively. These soft precipitating ions are likely produced by the parallel-energy dependent wave-particle interaction process initiated by the interaction of the hot ring current and cold plasmaspheric plasma in/near the plasmapause [*Williams and Lyons*, 1974]. Under this assumption the equatorward edge of the low-energy ion precipitation (~L=2.1) then also marks the ring current inner edge which can not be too far beyond the plasmapause.

Storm time ring current distributions are typically asymmetric and local time dependent [*Smith and Hoffman*, 1974; *Ejiri et al.*,

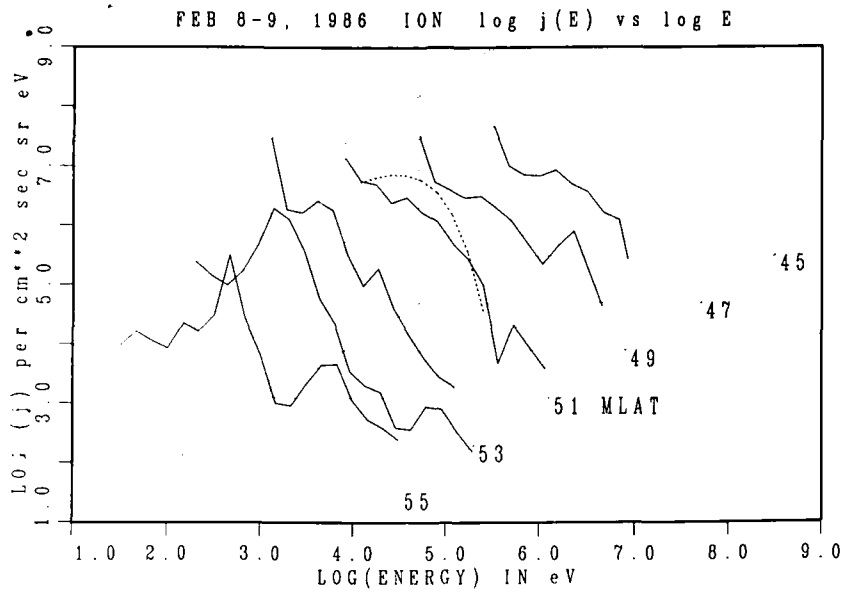

Fig. 8. Latitude variation of the ion energy spectra (directional differential number flux, in ions $cm^{-2}\,s^{-1}\,sr^{-1}\,eV^{-1}$) in and equatorward of the CPS. The energy of the peak flux varies with latitude, showing a dispersion feature between 55° and 51° MLAT. Spectra have a more thermal character at latitudes below 50° MLAT. A Maxwellian distribution function (with density ~30 cm^{-3} and temperature 120 eV) fit to the spectrum at 49° MLAT is denoted by the dashed curve.

1980]. During the increase of the convection electric field the ring current bulges toward the dayside [*Kivelson et al.*,1979; *Wolf et al.*, 1986]. The ring current density maximum in the postdusk sector is at a lower latitude than that in the predusk sector. In addition, evidence of storm time magnetic field distortion has been reported. *Lyons* [1979] has presented a case of magnetic field distortion at L=3-4 using simultaneous low- and high-altitude observations of ring current ions. He found that the magnetic field lines labeled L=3 at the Earth's surface near local midnight mapped to ~L=3.7 R_E in the equatorial plane during a period of enhanced magnetic activity if a quiet time magnetic field model were used. This implies a magnetic field configuration inflated by the enhanced ring current, with a stretch factor of 1.23 (3.7/3). In the magnetospheric equatorial plane the ring current-induced magnetic field distortion will have a stretching (compression) effect on the dipolar magnetic field lines outside (inside) of the ring current maximum. Thus a more realistic magnetic field configuration that takes the MLT dependence and the ring current magnetic field perturbation into consideration, would project the ionospheric foot print of the AMPTE observed ring current maximum to a lower latitude than that projected by the dipolar magnetic field mapping (see Figure 7). The more realistic magnetic field model should also project the latitude profile of the AMPTE observations with a sharper inner edge than that of the latitude profile presented in Figure 7. Based upon these arguments and from the ring current ion energy density profile measured by the AMPTE satellite at ~16.5 MLT, we suggest that the low-latitude ion drift peak measured by the Millstone radar at ~18.5 MLT is probably located on the same magnetic field line as that of the ring current density maximum, where the ring current effect on the electric field structure is most important.

Using the average energy and energy density distribution of the ring current O^+ and H^+ given by *Hamilton et al.* [1988], we estimate the Vasyliunas-Σ^*, the effective magnetospheric Hall conductivity. Combining Σ^* with the ionospheric Σ^H derived from the DMSP F6 precipitating electrons, we estimate the parameter Σ^*/Σ^H at the locations of the high-latitude (H) and low-latitude (L) westward ion drift peaks. The value of this parameter is 4 at the H latitude, and is 40 at the L latitude. This indicates the relative importance of the ring current particles in the two latitudes, and confirms our assertion that the low-latitude ion drift peak is controlled by ring current processes.

During the development of a storm main phase, energetic plasma is continuously injected into low-volume inner magnetic flux tubes (i.e., low L region). Sources and energization processes for the storm time injected particles have been discussed by many investigators [*Kivelson et al.*, 1979, and references therein]. Ions injected from the ionosphere [*Cladis and Francis*, 1985], ions convected from the plasma sheet and the geomagnetic tail, and the inward displaced preexisting trapped particles [*Lyons and Williams*, 1980] are the important sources of a storm's main phase ring current. Indeed, ions, principally O^+, of ionospheric origin constitute 67-80% of the inner ring current energy density near the maximum phase of the February 1986 storm [*Hamilton et al.*, 1988]. The accumulation of intense energetic ring current particles at very low L (<3) would result in a strong shielding effect to prevent the high-latitude electric field from penetrating to low latitude. Energetic ring current precipitation due to strong-pitch angle diffusion is inefficient this deep in the inner magnetosphere [*Williams and Lyons*, 1974] and the time scale for charge exchange loss is a few hours long. Thus plentiful energy density is available for driving azimuthal pressure gradients near the

inner edge of the ring current distribution during the main phase of a great magnetic storm. The dynamics of the great storm ring current energy distribution will be very different from those of substorms or moderate geomagnetic storms because the ring current sources and energization processes are different.

5. UT AND MLT VARIATIONS OF BOUNDARIES

From the coincident features of the ion convection, particle precipitation, and ring current distributions we have found that a correlation exists between the high-latitude ion drift peak and BPS-CPS transition boundary. The low-latitude ion drift peak falls between the precipitating electron and ion equatorward boundaries and is most probably collocated with the energetic ring current inner edge. In this section we discuss the temporal variations of these characteristic boundaries. We examine the consistency of these features and the evidence which supports our argument that the low-latitude ion drift peak is the low-altitude signature of the electric field shielding effect associated with ring current penetration into the outer layer of the storm time plasmasphere.

During the interval 2000 UT on February 8 to 0400 UT on February 9 there were five northern hemisphere passes of the DMSP F6 satellite in the dusk MLT sector, and of the DMSP F7 satellite in the premidnight MLT. Since local time dependence is important in the analysis of plasma regions, the approximate UT and MLT at 55° MLAT for each of the 10 DMSP passes are given in Table 1. During 2200 to 2400 UT on the 8th the Millstone radar was closer to the DMSP F6 satellite in local time, than to the DMSP F7 satellite. The reverse applies for the time interval between 0200 to 0400 UT on the 9th. We have examined the time-energy-number flux spectrograms of the precipitating particles observed by the two DMSP satellites to determine the precipitating particle transition and equatorward boundaries. Some gross features of the particle precipitation persisted throughout the six hours period (2100 UT February 8 - 0300 UT February 9) when the double-peaked ion drift patterns were observed, regardless of changing MLT (between 1800 and 2300 MLT). These included: (1) the precipitating ion equatorward boundary remained 5° to 10° lower than the electron equatorward boundary, (2) the ion energy-latitude dispersion feature (decreasing energy with decreasing latitude) was found just poleward of the ion equatorward boundary and soft precipitating ions (< 1 keV) occupied the rest of the region between the electron and ion boundaries, (3) near coincidence existed between the energetic ion (> 1 keV) equatorward boundary and the electron (30 eV-30 keV) equatorward boundary, and (4) intense energetic electrons constituted the boundary plasma sheet electron population and created conductivity gradients at the BPS/CPS transition boundaries.

The UT/MLT variations of the particle transition boundaries (TB), electron equatorward (EEB) and ion equatorward (IEB) boundaries derived from the satellite data are shown in Figure 9, along with the latitudes of the two peaks (H and L) in the ion convection patterns for comparison. In general, the separation between the electron and ion transition boundaries was insignificant. In spite of the low-time resolution (i.e., 101 min per orbit) and a 30-min time lag between the two satellite measurements, the three particle boundaries in the premidnight MLT sector are consistently lower than those at dusk. The DMSP F6 orbit at ~2035 UT and the DMSP F7 orbit at ~0400 UT were similar in local time (~2100 MLT). Comparing these two passes, the particle equatorward boundaries measured by both satellites show no significant UT variations. Their transition boundaries varied more sensitively with UT: lower TB latitude at 2035 UT, which was measured soon after the sudden IMF southward turning; higher TB during the decaying geomagnetic storm condition. As the radar observations rotated through local time (1500-2200 MLT), we can compare the radar observations with either the DMSP F6 observations or the DMSP F7 observations, whichever satellite is closer in the local time, to minimize the MLT effect.

TABLE 1. Satellite UT and MLT at 55° MLAT

DMSP F6		DMSP F7	
UT	MLT	UT	MLT
20.55	19.76	21.17	23.17
22.28	19.47	22.87	23.37
23.99	18.69	0.58	23.24
1.66	17.86	2.30	22.58
3.33	17.50	4.01	21.98

The latitude of the high-latitude ion drift peak (H) coincided well with the BPS/CPS transition boundary and H varied more sensitively with UT than did L. The low-latitude drift peaks (L) were consistently located equatorward of the plasma sheet electron precipitation (EEB) and poleward of the equatorward edge of the soft ion precipitation region (IEB) which may contain heated plasmaspheric ions. Thus the low-latitude ion drift peaks observed in the 1600-2200 MLT sector during the main and early recovery phases of the February storm, are strongly related to the inner edge of the ring current distribution. *Hamilton et al.* [1988] have reported that energetic H^+ (mean energy of 100 keV) and O^+ (mean energy of 75 keV) ions dominated the energy density in the inner ring current region near the storm maximum, and that the radial distance of the maximum ring current energy density slowly moved back out during the recovery of the February 1986 storm. They concluded that the rapid loss of O^+ through charge exchange was responsible for the fast initial recovery of the *Dst* (ring current strength) in a great storm. The nearly constant latitude location and the decreasing magnitude of the low-latitude ion drift peak with UT are consistent with the UT variations of the location and magnitude of the maximum ring current energy density at the radial distance L=2.5-3. This consistency suggests that the dynamics of the ring current pressure equatorward of the plasma sheet electron precipitation controlled the intensity and position of the low-latitude ion drift peak.

6. SUMMARY

We have presented a detailed analysis of the latitudinal structure of the *F* region ion convection observed with the Millstone Hill radar during the maximum phase of the great February 8-9, 1986, magnetic storm. The double-peaked (dual

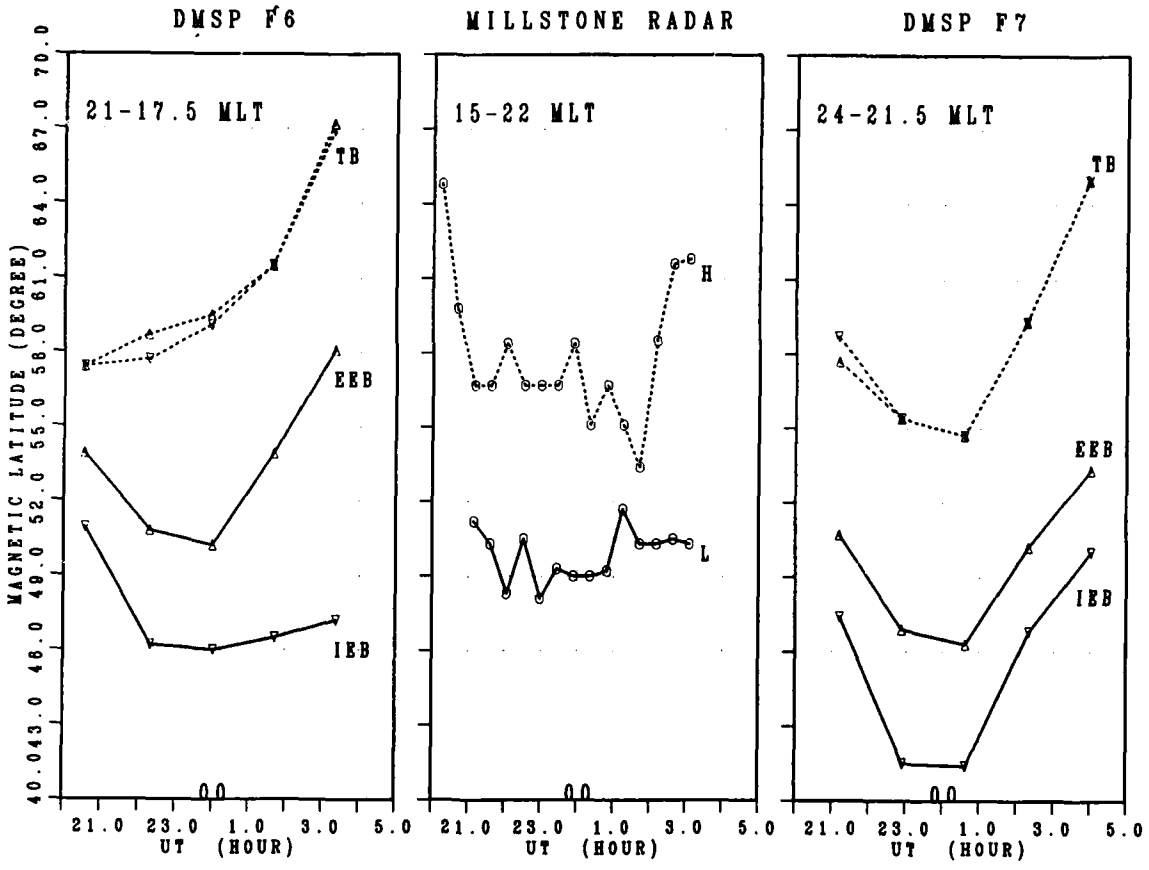

Fig. 9. UT variations of the latitudes of the high- (H) and low-latitude (L) westward ion drift maxima (middle panel), the particle BPS/CPS transition boundary (TB), and the electron and ion equatorward boundaries (EEB and IEB) at three magnetic local times from 2000 UT on the 8th to 0400 UT on the 9th. When the MLT difference is minimized, the high-latitude ion drift peaks (H) were collocated with TBs. The low-latitude ion drift peaks (L) varied slowly between the EEBs and IEBs.

maximum) westward ion drift (poleward electric field) pattern characterized the convection structure in the 1600-2200 MLT sector. The two peaks showed unrelated temporal variations, reflecting the time-scale difference in the processes (or sources) that controlled the electric field at the two latitudes. The latitude and magnitude of the high-latitude maximum varied more sensitively with UT than those of the low-latitude maximum. Temporal variations between the intensity of the low-latitude maximum and the *Dst* were found to be correlated.

Using simultaneous particle precipitation data from the DMSP F6 and F7 satellites, we have examined the low-altitude signatures of various magnetospheric plasma regions and determined the ionospheric conductivity distribution. We compared these particle features with the ion convection patterns and found the high-latitude (~57° Λ) westward ion drift peak to be collocated with the boundary plasma sheet-central plasma sheet (BPS-CPS) transition boundary, and the low-latitude (~49° Λ) drift peak to fall between the equatorward edges of the electron and soft ion precipitation. The high-latitude ion drift peak was associated with conductivity gradients embedded in the high conductivity region, while the low-latitude ion drift peak was located in the low conductivity region.

Based upon the ion energy-latitude dispersion signature and precipitating ion spectral characteristics, we find evidence for the presence of heated plasmaspheric ions in the vicinity of the low-latitude ion drift peak. Thus we argue that the low-latitude ion drift peak was located inside the plasmapause. Furthermore, combining these low-altitude observations with simultaneous ring current observations from the AMPTE satellite in the equatorial magnetosphere [*Hamilton et al.*,1988], we find that the latitude and magnitude variations of the low-latitude ion drift peak are closely related to those of the maximum of the O^+ ring current-dominated energy density distribution. These findings lead us to conclude that the intense electric field observed at ~49°Λ in the low conductivity region, is driven by asymmetric energetic ring current ions which penetrated beyond the plasma sheet inner edge and/or plasmapause.

The shielding effect resulting from the ring current particle distribution can significantly modify the magnetosphere-ionosphere electric field structure. In a low conductivity region, ionospheric current closure of the field-aligned currents driven by the ring current pressure gradients requires the existence of an intense electric field. Significant differences in the ring current source and location exist between a great storm and moderate storm or substorm conditions. Ions of ionospheric origin, which dominate the inner ring current population, are an unique feature during great magnetic storms. Thus under great

storm conditions the dynamics (production, transport and loss) of ring current particles at its inner edge should be very different from that of particles of magnetospheric origin at higher latitudes. We suggest that the uncorrelated UT/MLT variation of the high-latitude ion drift peak and the low-latitude ion drift peak mirrors such a decoupling of features between the inner and the outer magnetosphere.

Acknowledgments. The Millstone Hill radar program is supported by National Science Foundation cooperative agreement ATM-88-08137 and a portion of the analysis activities at Millstone Hill is supported by the U.S. Air Force Office of Scientific Research through grant AFOSR-89-0454 to the Massachusetts Institute of Technology. We acknowledge many helpful discussions with the members of the Atmospheric Science group at Millstone Hill and thank D. E. Madden and J. James for organizing the DMSP satellite particle and field data. The analysis of DMSP data by GL personnel is supported by the U.S. Air Force Office of Scientific Research Task 2311G5.

The Editor thanks O. de la Beaujardiere and C. Senior for their assistance in evaluating this paper.

REFERENCES

Basu, B., J. R. Jasperse, R. M. Robinson, R. R. Vondrak, and D. S. Evans, Linear transport theory of auroral proton precipitation: A comparison with observations, *J. Geophys. Res.*, *92*, 5920, 1987.

Blanc, M., Mid-latitude convection electric fields and their relation to ring current development, *Geophys. Res. Lett.*, *5*, 203, 1978.

Blanc, M., Magnetospheric convection effects at mid-latitudes, 3, Theoretical derivation of the disturbance convection pattern in the plasmasphere, *J. Geophys. Res.*, *88*, 235, 1983.

Blanc, M., and A. D. Richmond, The ionospheric disturbance dynamo, *J. Geophys. Res.*, *85*, 1669, 1980.

Chen, A. J., Penetration of low-energy protons deep into the magnetosphere, *J. Geophys. Res.*, *75*, 2458, 1970.

Cladis, J. B., and W. E. Francis, The polar ionosphere as a source of the storm time ring current, *J. Geophys. Res.*, *90*, 3465, 1985.

Cornwall, J. M., F. V. Coroniti, and R. M. Thorne, Turbulent loss of ring current protons, *J. Geophys. Res.*, *75*, 4699, 1970.

Cowley, S.W.H., and M. Ashour-Abdalla, Adiabatic plasma forbidden-zone effects for a simple electric field model, *Planet. Space Sci.*, *24*, 821, 1976.

Doyle, M. A., W. J. Burke, D. A. Hardy, P. F. Bythrow, F. J. Rich, and T. A. Potemra, A simple model of auroral electrodynamics compared with HILAT measurements, *J. Geophys. Res.*, *91*, 6979, 1986.

Ejiri, M., Trajectory traces of charged particles in the magnetosphere, *J. Geophys. Res.*, *83*, 4798, 1978.

Ejiri, M., R. A. Hoffman, and P. H. Smith, Energetic particle penetrations into the inner magnetosphere, *J. Geophys. Res.*, *85*, 653, 1980.

Foster, J. C., Plasma transport through the dayside cleft: A source of ionization patches in the polar cap, in *Electromagnetic Coupling in the Polar Clefts and Caps*, edited by P. E. Sandholt and A. Egeland, pp. 343-354,Kluwer, Boston, 1989.

Foster, J. C., C. G. Park, L. H. Brace, J. R. Burrows, J. H. Hoffman, E. J. Maier, and J. H. Whitteker, Plasmapause signatures in the ionosphere and magnetosphere, *J. Geophys. Res.*, *83*, 1,175, 1978.

Foster, J. C., J. M. Holt, R. G. Musgrove, and D. S. Evans, Ionospheric convection associated with discrete levels of particle precipitation, *Geophys. Res. Lett.*, *13*, 656, 1986.

Foster, J. C., H.-C Yeh, R. A. Eastes, and F. J. Rich, Radar/satellite observations of nightside auroral boundaries, *Eos Trans. AGU*, *70*, 1239, 1989.

Foster, J. C., H.-C. Yeh, J. A. Klobuchar, and W. Swider, Millstone Hill observations of storm-related ionospheric perturbations at mid-latitudes, *Eos Trans. AGU*, *71*, 610, 1990.

Gussenhoven, M. S., D. A. Hardy, and N. Heinemann, The equatorward boundary of auroral ion precipitation, *J. Geophys. Res.*, *92*, 3273, 1987.

Hamilton, D. C., G. Gloeckler, F. M. Ipavich, W. Studemann, B. Wilken, and G. Kremser, Ring current development during the great geomagnetic storm of February 1986, *J. Geophys. Res.*, 93, 14,343, 1988.

Hardy, D. A., L. K. Schemitt, M.S. Gussenhoven, F. J. Marshall, H.-C. Yeh, T. L. Schumaker, A. Huber, and J. Pantazis, Precipitating electron and ion detectors (SSJ/4) for the block 5D/flights 6-10 DMSP satellites: Calibration and data presentation, *Rep. AFGL Tech. Rep., 84 0317, Air Force Geophys. Lab.*, Hanscom Air Force Base, Mass., 1984.

Harel, M., R. A. Wolf, P. H. Reiff, R. W. Spiro, W. J. Burke, F. J. Rich, and S. M. Smiddy, Quantitative simulation of a magnetospheric substorm, 1, Model logic and overview, *J. Geophys. Res.*, *86*, 2217, 1981.

Holt, J. M., R. H. Wand, and J. V. Evans, Millstone Hill measurements on 26 February 1979 during the solar eclipse and formation of midday *F* region trough, *J. Atmos. Terr. Phys.*, *46*, 251, 1984.

Jaggi, R. K., and R. A. Wolf, Self-consistent calculation of the motion of a sheet of ions in the magnetosphere, *J. Geophys. Res.*, *78*, 2852, 1973.

Kavanagh, L. D., Jr., J. W. Freeman, Jr., and A. J. Chen, Plasma flow in the magnetosphere, *J. Geophys. Res.*, *73*, 5511, 1968.

Kennel, C. F., Consequences of a magnetospheric plasma, *Rev. Geophys.*, *7*, 379, 1969.

Kivelson, M. G., S. M. Kaye, and D. J. Southward, The physics of plasma injection events, in *Dynamics of the Magnetosphere*, edited by S.-I. Akasofu, pp. 385-405, D. Reidel, Hingham, Mass., 1979.

Lyons, L. R., Magnetic field distortions at $L=3$-4 inferred from simultaneous low and high altitude observations of ring current ions, in *Quantitative Modeling of Magnetospheric Processes, Geophys. Monogr. Ser.*, vol. 21, p. 64, edited by W. P. Olson, AGU, Washington, D. C., 1979.

Lyons, L. R., and D. J. Williams, A source for the magnetospheric storm main phase ring current, *J. Geophys. Res.*, *85*, 523, 1980.

Providakes, J. F., M. C. Kelley, W. E. Swartz, M. Mendillo, and J. M. Holt, Radar and optical measurements of ionospheric processes associated with intense subauroral electric fields, *J. Geophys. Res.*, *94*, 5350, 1989.

Rich, F. J., W. J. Burke, M. C. Kelley, and M. Smiddy, Observations of field-aligned currents in association with strong convection electric fields at subauroral latitudes, *J. Geophys. Res.*, *85*, 2335, 1980.

Robinson, R. M., R. R. Vondrak, K. Miller, T. Dabbs, and D. Hardy, On calculating ionospheric conductances from the flux and energy of precipitating electrons, *J. Geophys. Res.*, *92*, 2565, 1987.

Schield, M. A., J. W. Freeman, and A. J. Dessler, A source for field-aligned currents at auroral latitudes, *J. Geophys. Res.*, *74*, 247, 1969.

Senior, C., and M. Blanc, On the control of magnetospheric convection by the spatial distribution of ionospheric conductivities, *J. Geophys. Res. 89*, *261*, 1984.

Senior, C., J. R. Sharber, O. de la Beaujardiere, R. A. Heelis, D. S. Evans, J. D. Winningham, M. Sugiura, and W. R. Hoegy, *E* and *F* region study of the evening sector auroral oval: A Chatanika/Dynamics Explorer 2/NOAA 6 Comparison, *J. Geophys. Res. 92*, 2477, 1987.

Siscoe, G. L., Energetic coupling between region 1 and 2 Birkeland current systems, *J. Geophys. Res.*, *87*, 5124, 1982.

Smiddy, M., M. C. Kelly, W. Burke, F. Rich, R. Sagalyn, B. Schman, R. Hays, and S. Lai, Intense poleward-directed electric fields near the ionospheric projection of the plasmapause, *Geophys. Res. Lett.*, *4*, 543, 1977.

Smith, P. H., and R. A. Hoffman, Direct observations in the dusk hours of the characteristics of the storm time ring current particles during the beginning of magnetic storms, *J. Geophys. Res.*, *79*, 966, 1974.

Southwood D. J., and R. A. Wolf, An assessment of the role precipitation in magnetospheric convection, *J. Geophys. Res.*, *83*, 5227, 1978.

Spiro, R. W., R. A. Heelis, and W. B. Hanson, Rapid subauroral ion drifts observed by Atmospheric Explorer C, *Geophys. Res. Lett.*, *6*, 657, 1979.

Spiro, R. W., R. A. Wolf, and B. G. Fever, Penetration of high-latitude electric-field effects to low latitudes during SUNDIAL 1984, *Ann. Geophys.*, *6*, 39-50, 1988.

Swider, W., Precipitating and trapped ions and electrons observed at 840 km during the great magnetic storm of February, 1986, *J. Geophys. Res.*, *95*, 10417, 1990.

Swift, D. W., Possible consequences of the asymmetric development of the ring current belt, *Planet. Space Sci.*, *15*, 835, 1967.

Tsyganenko, N. A., Quantitative models of the magnetospheric magnetic field: Methods and results, *Space Sci. Rev.*, *54*, 75, 1990.

Magnetosphere, edited by B. M. McCormac, p. 60, D. Reidel, Hingham, Mass., 1970.

Vasylinuas, V. M., The interrelationship of magnetospheric processes,

in *Earth's Magnetospheric Processes*, edited by B. M. McCormac, p. 29, D. Reidel, Hingham, Mass., 1972.

Williams, D. J., and L. R. Lyons, The proton ring current and its interaction with the plasmapause: Storm recovery phase, *J. Geophys. Res.*, *79*, 4195, 1974.

Winningham, J. D., F. Yasuhara, S.-I. Akasofu, and W. J. Heikkila, The latitudinal morphology of 10-eV to 10-keV electrons fluxes during magnetically quiet and disturbed times in the 2100-0300 MLT sector, *J. Geophys. Res.*, *80*, 3148, 1975.

Wolf, R. A., Effects of ionospheric conductivity on convective flow of plasma in the magnetosphere, *J. Geophys. Res.*, *75*, 4677, 1970.

Wolf, R. A., M. Harel, R. W. Spiro, G. -H. Voigt, P. H. Reiff, and C. K. Chen, Computer simulation of inner magnetospheric dynamics for the magnetic storm of July 29, 1977, *J. Geophys. Res. 87*, 5949, 1982.

Wolf, R. A., R. W. Spiro, and G. A. Mantjoukis, Theoretical comments on the nature of the plasmapause, *Adv. Space Res.*, *6*, 177, 1986.

Yeh, H.-C., and J. C. Foster, Storm time heavy ion outflow at mid-latitude, *J. Geophys. Res.*, *95*, 7881, 1990.

Yeh, H.-C., J. C. Foster, J. M. Holt, R. H. Redus, and F. J. Rich, Radar and Satellite observations of the storm time cleft, *J. Geophys. Res.*, *95*, 12,075, 1990.

J. C. Foster and H.-C. Yeh, Atmospheric Sciences Group, M.I.T. Haystack Observatory, Westford, MA 01886.

F. J. Rich and W. Swider, Space Physics Division, Geophysics Laboratory, Hanscom AFB, MA 01731.

(Received August 27, 1990;
revised December 10, 1990;
accepted December 11, 1990.)